Tuning Co-Ni Electrochemical Active Sites via Iron Incorporation in Carbonate Hydroxide Frameworks for High-Performance Supercapacitors

Dwititapa Mohanty[a], Trupti Tanaya Mishra[a], Sudhansu B Barik[a], Ankita Dey[b], R. Thangavel[b], , Santosh Kumar Mishra[c], Dhrubojyoti Roy[#a], Mohua Chakraborty*[a]

[a]Department of Physics, C. V. Raman Global University, Bhubaneswar, Odisha-752054, India.
[b]Department of Physics, IIT(ISM), Dhanbad, Jharkhand 826004, India.
[C]School of Chemical Sciences, National Institute of Science Education and Research, Bhubaneswar, Jatni, Khurda, Odisha, 752050, India.
*Corresponding E-mail: mchakraborty1988@gmail.com.
#Corresponding E-mail: dhrubojyoti27@gmail.com.

We have tested the pH value of solutions in each possible steps of reactions for all nine samples as follows:

Table S1: pH value of solutions in each possible steps of reactions

Sample	Nickel Nitrate and Cobalt Nitrate before hydrothermal	Nickel Nitrate, Cobalt Nitrate and Iron Nitrate before hydrothermal	Containing Nickel Nitrate, Cobalt Nitrate, (Iron Nitrate) and Urea before hydrothermal	ontaining Nickel Nitrate, Cobalt Nitrate, Iron Nitrate and Urea after hydrothermal
NiCo-CH	≈ 6.2	NA	≈ 6.2	≈ 8.9
$Fe_{0.05}Co_{0.95}Ni$-CH	≈ 6.1	≈ 5.9	≈ 5.9	≈ 7.5
$Fe_{0.1}Co_{0.90}Ni$-CH	≈ 6.1	≈ 5.2	≈ 5.2	≈ 7.3
$Fe_{0.15}Co_{0.85}Ni$-CH	≈ 6.0	≈ 4.9	≈ 4.9	≈ 7.2
$Fe_{0.2}Co_{0.80}Ni$-CH	≈ 6.0	≈ 4.8	≈ 4.8	≈ 7
$Fe_{0.05}Ni_{0.95}Co$-CH	≈ 6.3	≈ 5.9	≈ 5.9	≈ 7.9
$Fe_{0.1}Ni_{0.90}Co$-CH	≈ 6.2	≈ 5.3	≈ 5.3	≈ 7.8
$Fe_{0.15}Ni_{0.85}Co$-CH	≈ 6.1	≈ 5.1	≈ 5.1	≈ 7.5
$Fe_{0.2}Ni_{0.80}Co$-CH	≈ 6.1	≈ 4.9	≈ 4.9	≈ 7.1

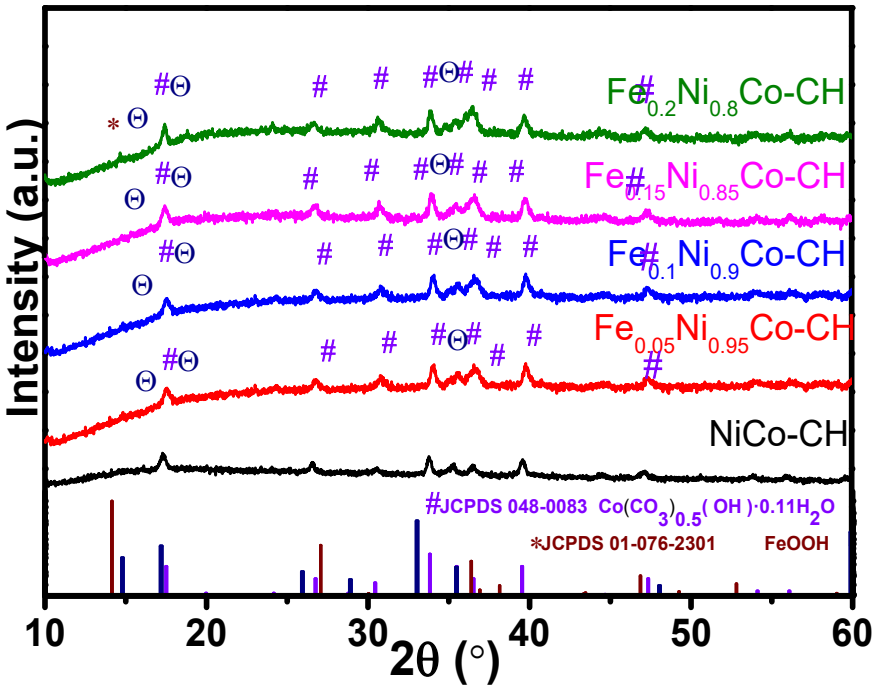

Fig. S1: XRD pattern of $Fe_xNi_{(1-x)}CoCH$ samples in zoomed view.

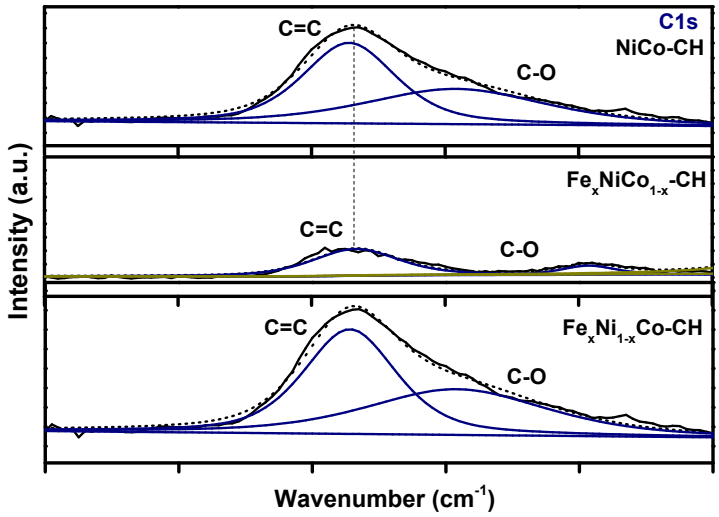

Fig. S2: High-resolution narrow scan XPS spectra for C1s of the as-prepared NiCo-CH, $Fe_{0.1}Co_{0.9}Ni$-CH and $Fe_{0.05}Co_{0.95}Ni$-CH materials.

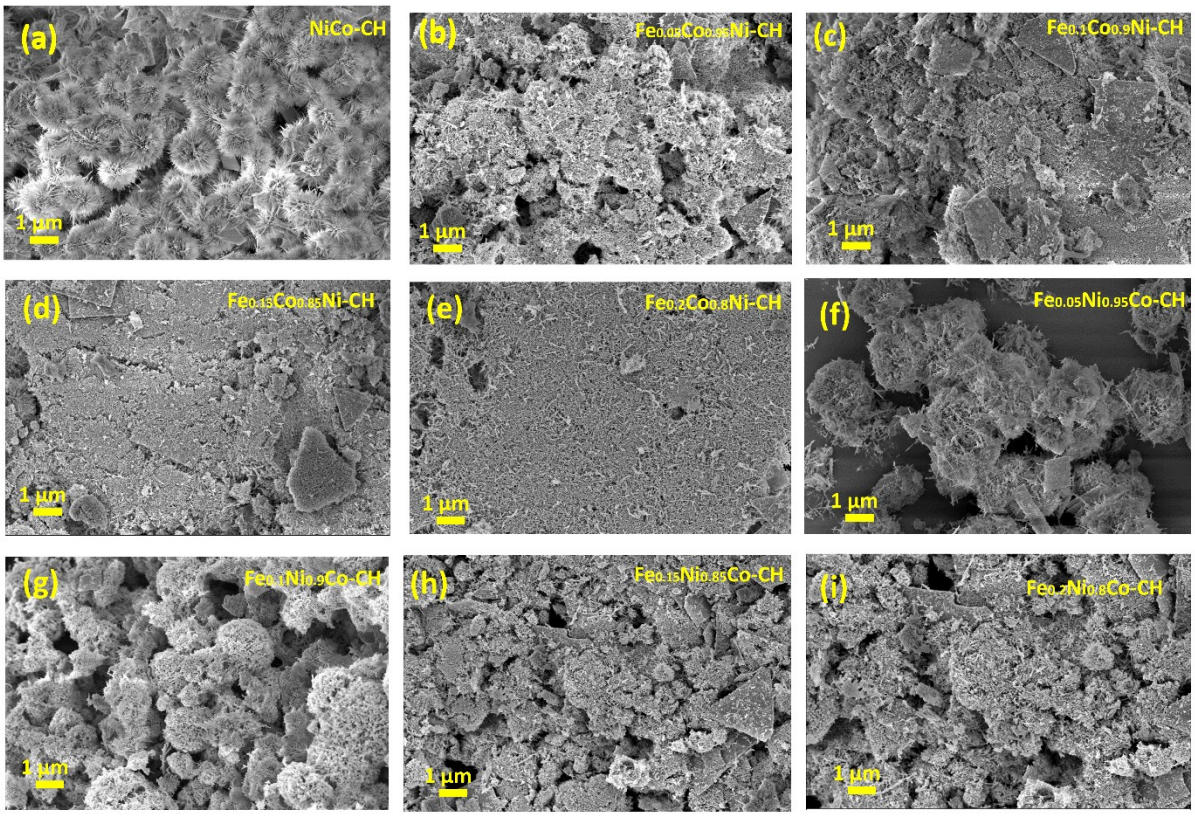

Fig. S3: SEM images of (a) NiCo-CH (b-e) $Fe_xCo_{(1-x)}Ni$-CH (f-i) $Fe_xNi_{(1-x)}Co$-CH samples

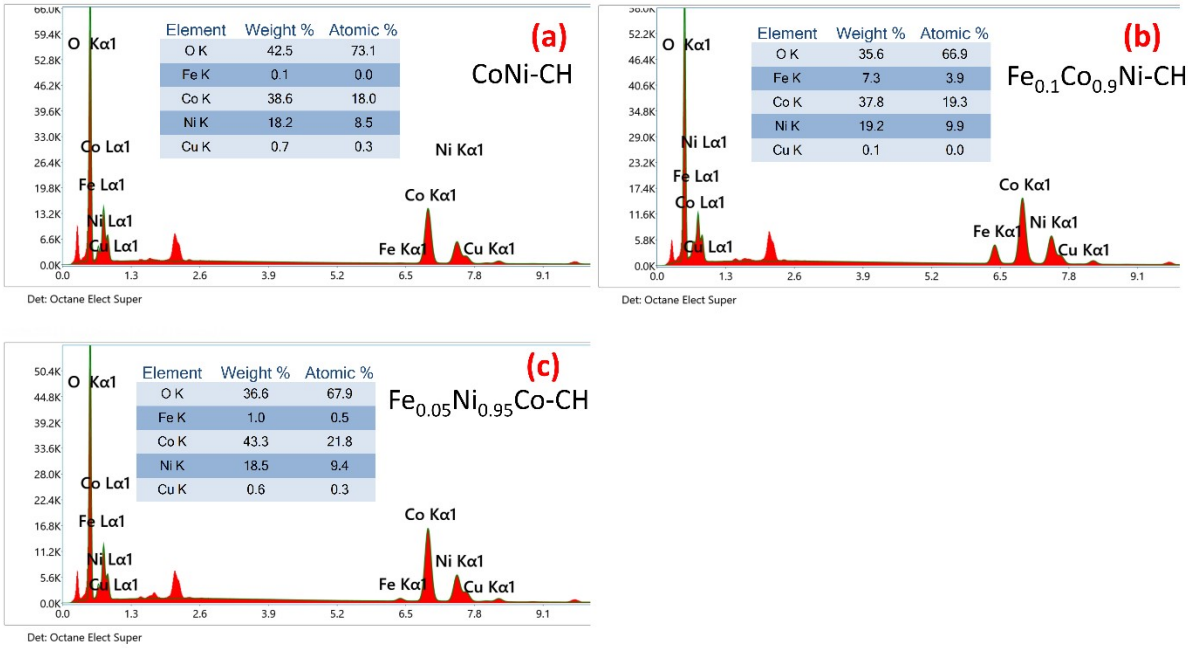

Fig. S4: EDAX data of (a) NiCoCH (b) $Fe_{0.1}Co_{0.9}Ni$-CH (c) $Fe_{0.05}Ni_{0.95}Co$-CH samples

In EDAX pattern, the small Cu signal (~0.7 wt%) observed in Fig. S4 is most likely due to trace contamination from the copper SEM grid or instrumental background during analysis rather than from the synthesis process itself.

Table S2 : ICP-AES data of optimized samples

Sample	Element	Concentration in ppm	Weight of element	sample weight	Weight (%)
$Fe_{0.05}Ni_{0.95}Co$-CH	Ni	13.744	0.6872	4.9	14.0244898
	Co	34.364	1.7182	4.9	35.0653061
	Fe	0.912	0.0456	4.9	0.93061224
$Fe_{0.1}Co_{0.90}Ni$-CH	Ni	7.821	0.39105	2.3	17.0021739
	Co	16.272	0.8136	2.3	35.3739130
	Fe	0.985	0.04925	2.3	2.14130434
NiCo-CH	Ni	18.018	0.9009	4.7	19.1680851
	Co	33.905	1.69525	4.7	36.0691489

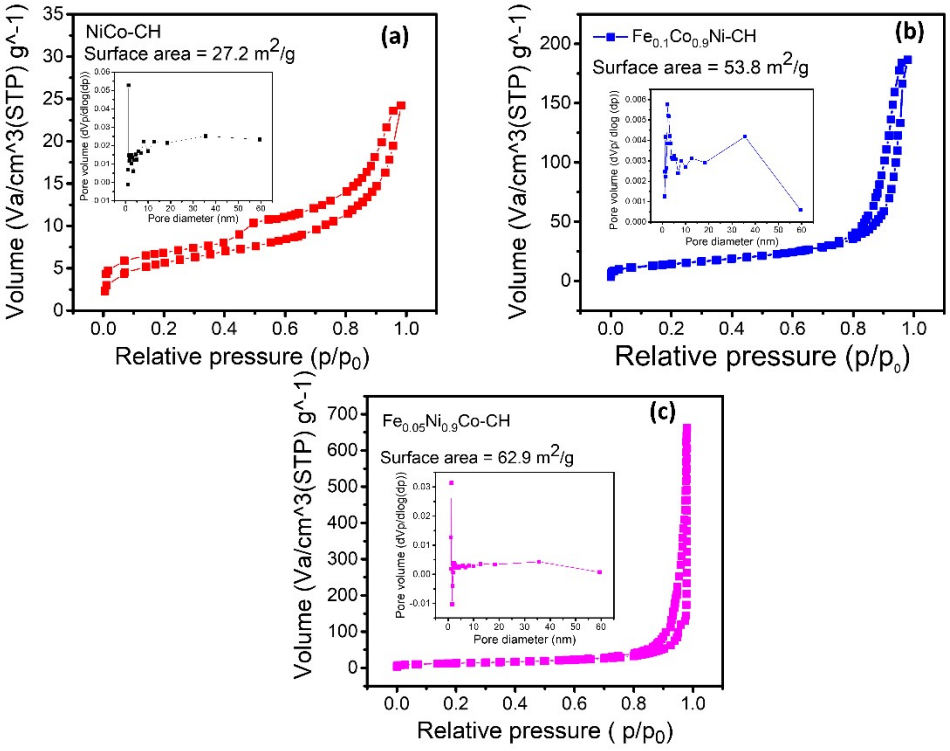

Fig. S5: BET measurement for (a) NiCo-CH (b) $Fe_{0.1}Co_{0.9}Ni$-CH (c) $Fe_{0.05}Ni_{0.95}Co$-CH samples, *in inset* pore volume-pore diameter, respectively.

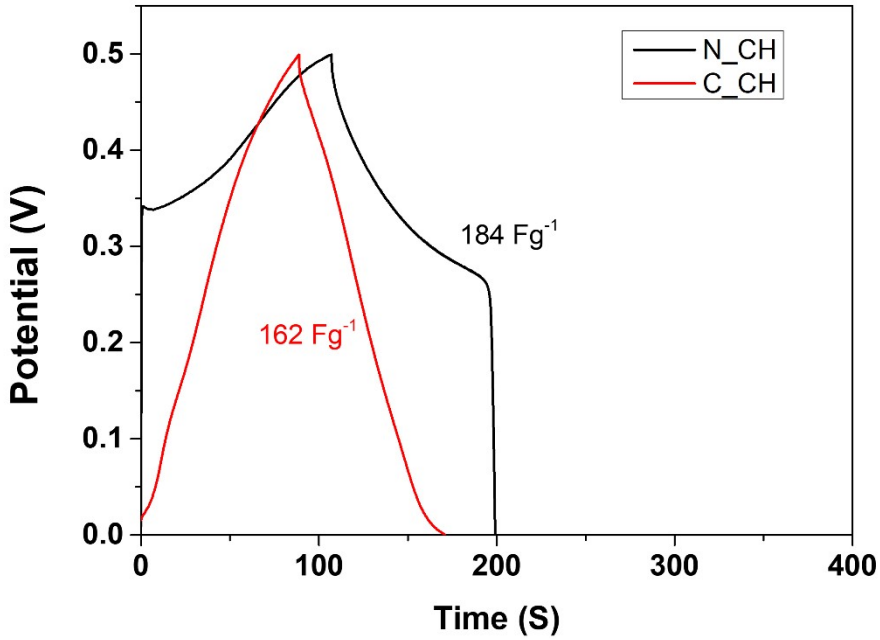

Fig. S6: GCD plot of Ni-CH and Co-CH at 2mVs^{-1}.

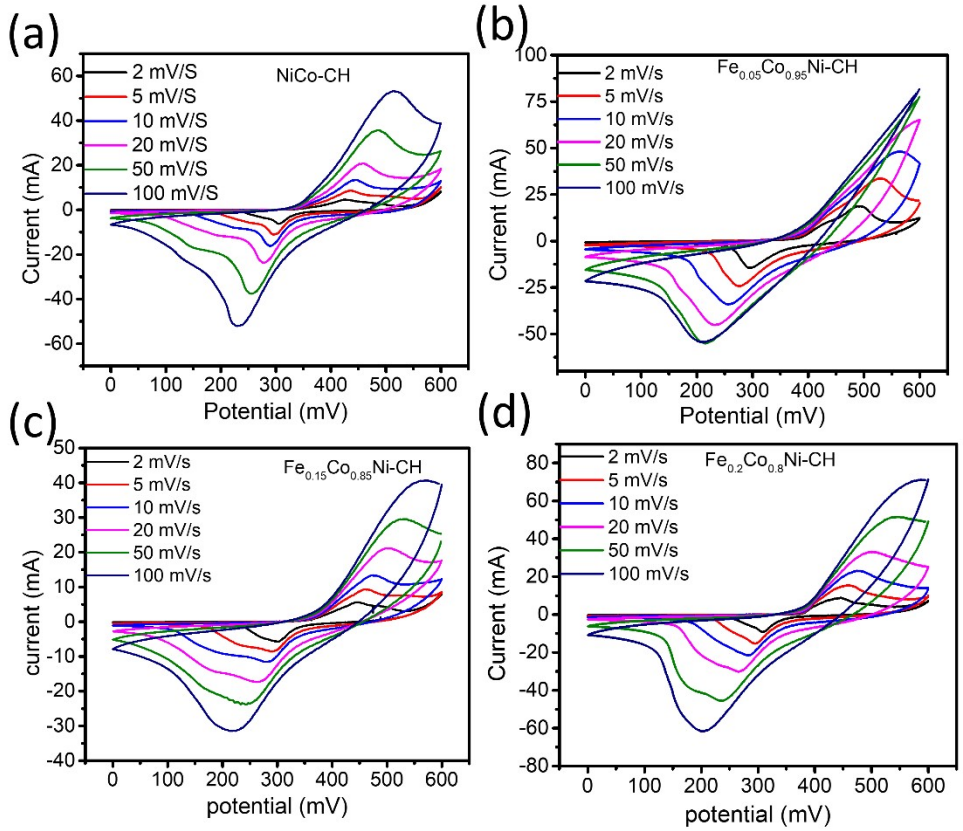

Fig. S7: CV plots of (a) NiCo-CH, (b) $Fe_{0.05}Co_{0.95}Ni$-CH (c) $Fe_{0.15}Co_{0.85}Ni$-CH (d) $Fe_{0.2}Co_{0.8}Ni$-CH at different scan rates

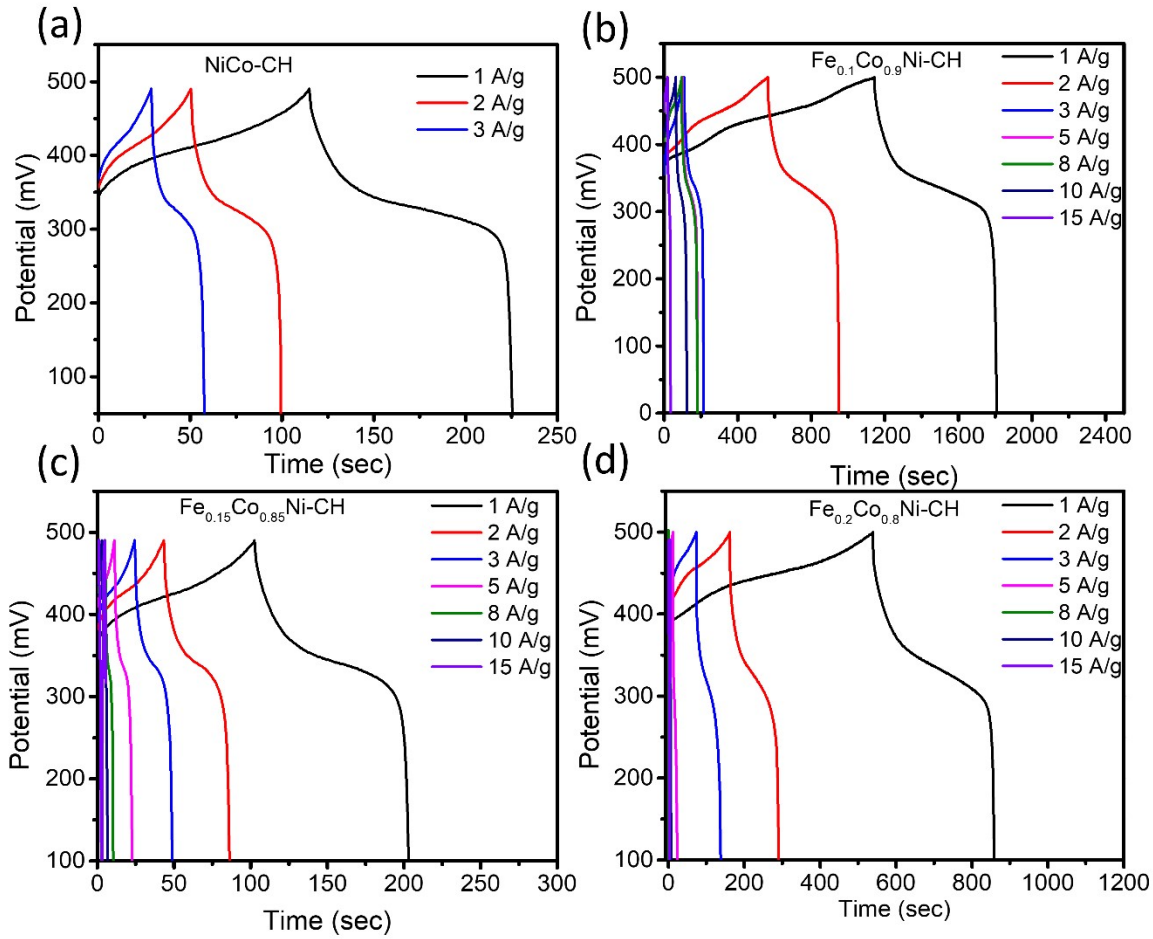

Fig. S8: GCD profiles of (a) NiCo-CH, (b) $Fe_{0.05}Co_{0.95}Ni$-CH (c) $Fe_{0.15}Co_{0.85}Ni$-CH (d) $Fe_{0.2}Co_{0.8}Ni$-CH at different current densities

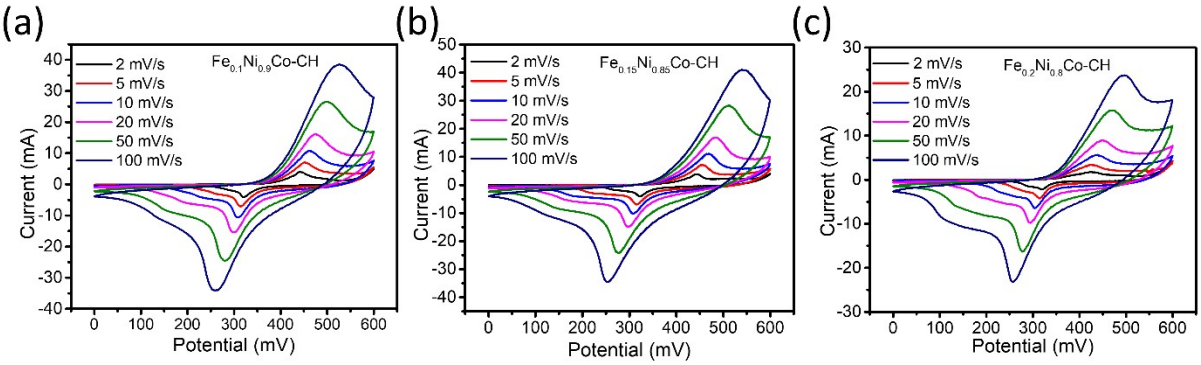

Fig. S9: CV plots of (a) $Fe_{0.1}Ni_{0.9}Co$-CH (b) $Fe_{0.15}Ni_{0.85}Co$-CH (c) $Fe_{0.2}Ni_{0.8}Co$-CH at different scan rates

Table S3: Electrochemical super capacitive parameters of synthesized samples						
Sample	**Csp (GCD) Fg^{-1}**	**b value**	**R_s (Ω)**	**R_{ct} (Ω)**	**CPE1 ($mF{\cdot}cm^{-2}S$)**	**CPE2 ($mF{\cdot}cm^{-2}S$)**
NiCo-CH	424	0.51	1.48	18.864	16.34	64.79
$Fe_{0.05}Co_{0.95}$Ni-CH	895	0.29	0.48	2.81	25.41	1.406
$Fe_{0.1}Co_{0.90}$Ni-CH	1080	0.45	2.5	4.72	121	312
$Fe_{0.15}Co_{0.85}$Ni-CH	804	0.92	1.8	10.06	7.76	695.84
$Fe_{0.2}Co_{0.80}$Ni-CH	841	0.88	0.39	3.22	25.82	1.12
$Fe_{0.05}Ni_{0.95}$Co-CH	2898	0.83	2.16	0.769	555	670
$Fe_{0.1}Ni_{0.90}$Co-CH	1606	0.56	2.5	10.92	120.5	252.3
$Fe_{0.15}Ni_{0.85}$Co-CH	423	0.52	3.96	22.30	215	128
$Fe_{0.2}Ni_{0.80}$Co-CH	216	0.25	8.24	9.39	15.23	40.34

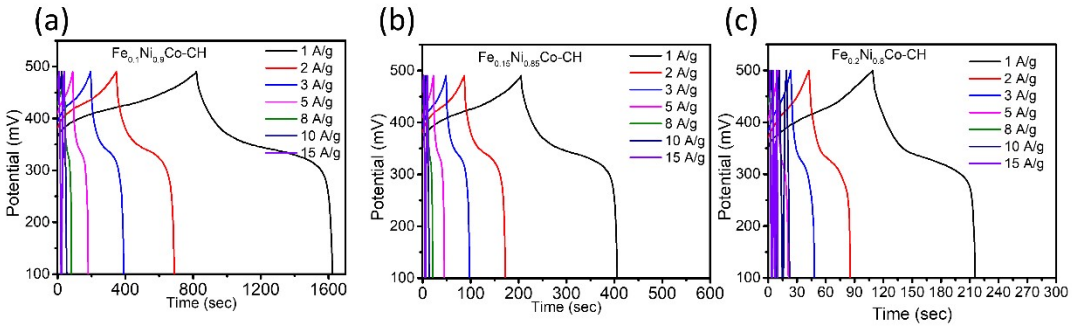

Fig. S10: GCD profiles of (a) $Fe_{0.1}Ni_{0.9}$Co-CH (b) $Fe_{0.15}Ni_{0.85}$Co-CH (c) $Fe_{0.2}Ni_{0.8}$Co-CH at different current densities

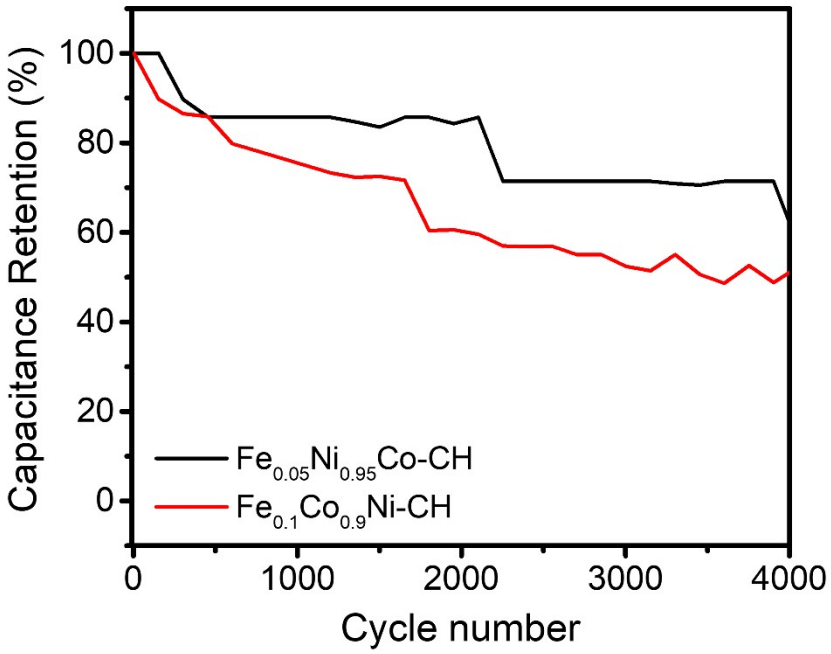

Fig. S11: Cyclic stability of $Fe_{0.1}Co_{0.9}$Ni-CH and $Fe_{0.05}Ni_{0.95}$Co-CH at current densities 10 A/g.

Table S4: Literature Comparison for Supercapacitance Performance

Electrode Material	Morphology	Specific Capacitance	Reference
NiCoFe-LDH	Nanocomposite	3130 F/g at 1A/g	[1]
Ni4/Co1(OH)2	Nanostructure	1820 F/g at 1A/g	[2]
Fe-Co Hydroxide (1:1 ratio)	—	2255.6 F/g at 1A/g	[3]
NiCo-CH (CH-S3)	Layered	2130 F/g (at 2 A/g)	[4]
CoNiFe-LDH/CNFs-0.5	Nanofibers	1203 F/g	[5]
NiCo-CH-180	Nanorods	762 F/g at 1A/g	[6]
NiCo-LDH	Nanosheets	1470 F/g	[7]
$Fe_xCo_{(1-x)}$Ni-CH (Optimized)	Nanorods (w/ FeOOH)	1080 F/g at 1/A/g	**Our Work**
$Fe_xNi_{(1-x)}$Co-CH (Optimized)	Nanorods	2898 F/g at 1A/g	**Our Work**

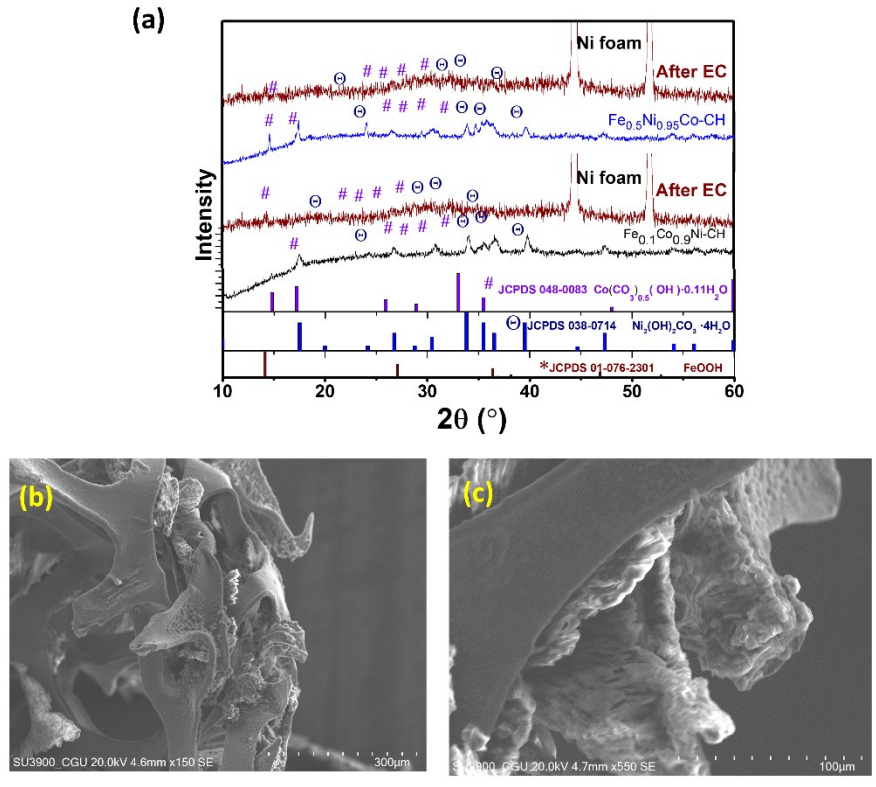

Fig. S12: (a) XRD pattern for $Fe_{0.1}Co_{0.9}$Ni-CH and $Fe_{0.05}Ni_{0.95}$Co-CH after electrochemical cycling stability, (b) and (c) SEM images of $Fe_{0.1}Co_{0.9}$Ni-CH and $Fe_{0.05}Ni_{0.95}$Co-CH post electrochemical cycling respectively.

References:

(1) Pourfarzad, H.; Shabani-Nooshabadi, M.; Ganjali, M. R.; Kashani, H. Synthesis of Ni–Co-Fe Layered Double Hydroxide and Fe2O3/Graphene Nanocomposites as Actively Materials for High Electrochemical Performance Supercapacitors. *Electrochimica Acta* **2019**, *317*, 83–92. https://doi.org/10.1016/j.electacta.2019.05.122.

(2) Li, H.; Zhou, X.; Zhao, P. Amorphous Ni–Co Binary Hydroxide with Super-Long Cycle Life and Ultrahigh Rate Capability as Asymmetric Supercapacitors. *Nanotechnology* **2023**, *34* (6), 065703. https://doi.org/10.1088/1361-6528/aca1cb.

(3) Jiang, L.; Sui, Y.; Qi, J.; Chang, Yuan.; He, Y.; Meng, Q.; Wei, F.; Sun, Z.; Jin, Y. Structure Dependence of Fe-Co Hydroxides on Fe/Co Ratio and Their Application for Supercapacitors. *Part & Part Syst Charact* **2017**, *34* (2), 1600239. https://doi.org/10.1002/ppsc.201600239.

(4) Lim, H.; Park, Y. S.; Baek, S. Structure and Electrochemical Performances of NiCo Hydroxide with Anion Exchange by Carbonates for Hybrid Supercapacitor. *J Am Ceram Soc.* **2025**, *108* (10), e70061. https://doi.org/10.1111/jace.70061.

(5) Wang, F.; Sun, S.; Xu, Y.; Wang, T.; Yu, R.; Li, H. High Performance Asymmetric Supercapacitor Based on Cobalt Nickle Iron-Layered Double Hydroxide/Carbon Nanofibres and Activated Carbon. *Sci Rep* **2017**, *7* (1), 4707. https://doi.org/10.1038/s41598-017-04807-1.

(6) Kumar, S.; Satpathy, B. K.; Pradhan, D. Morphology-Controlled Synthesis of a NiCo-Carbonate Layered Double Hydroxide as an Electrode Material for Solid-State Asymmetric Supercapacitors. *Mater. Adv.* **2024**, *5* (6), 2271–2284. https://doi.org/10.1039/D3MA01008B.

(7) Kumar, S.; Pradhan, D. Binder- and Additive-Free Electrophoretic Deposition of Solvothermally Synthesized Nickel–Cobalt Layered Double Hydroxide for High-Performance Asymmetric Solid-State Supercapacitor. *ACS Appl. Energy Mater.* **2025**, *8* (13), 9878–9890. https://doi.org/10.1021/acsaem.5c01703.